Improvement of AMSR2 Soil Moisture Retrieval Using a Soil-Vegetation Temperature Decomposition Algorithm

Xiangjin Meng, *Student Member, IEEE*, Yingbao Yang, Jiangyuan Zeng, *Senior Member, IEEE*, Jian Peng, *Senior Member, IEEE*, and Jia Hu

***Abstract*—It is well documented that soil moisture can be retrieved from passive microwave observations. A basic assumption of most passive microwave-based soil moisture retrieval algorithms is that vegetation temperatures (Tv) and soil temperatures (Ts) are equal (i.e., Tv=Ts), which however is not well satisfied in some cases, especially during daytime. In this study, we proposed a soil-vegetation temperature decomposition (SVTD) approach to avoid such an assumption, which can improve the accuracy of soil moisture retrievals from the Advanced Microwave Scanning Radiometer 2 (AMSR2) data. First, the SVTD was used to decompose the vegetation and soil temperatures of the soil-vegetation mixed pixels in the Tibetan Plateau (TP). Subsequently, the decomposed temperature was integrated into the soil moisture retrieval algorithm to correct the effects of soil and vegetation temperatures, and soil moisture is then retrieved following the same strategy adopted in the land parameter retrieval model (LPRM). Finally, the algorithm was validated against densely-instrumented soil moisture networks (Maqu, Naqu, and Ngari) built in the Tibetan Plateau, and was also compared with the LPRM AMSR2 soil moisture product. Results indicate the proposed algorithm performs much better than the original LPRM in soil-vegetation mixed areas. The proposed SVTD method is promising for soil moisture retrieval from passive microwave satellites, especially in the daytime when the difference between soil and vegetation temperatures is relatively large.**

***Index Terms*—Soil moisture, Temperature decomposition, AMSR2, Passive microwave, LPRM**

I. Introduction

SOIL moisture (SM) is an important state variable in the water, energy, and carbon cycles [1]. Passive microwave (PMW) remote sensing (RS) has been recognized as an indispensable avenue to detect SM at global and continent scales [2]. The primary advantage of PMW sensors for SM mapping is that they are capable of working under cloudy weather and nighttime, and are less sensitive to surface roughness and vegetation cover [3]. The physical basis of SM estimated from PMW observations is that brightness temperature (TB) acquired from PMW is closely related to soil permittivity, which is mainly determined by SM [4]-[6]. In addition, the TB consists of signal contributions from the soil and the overlying vegetation temperatures, surface roughness, and vegetation canopy, which need to be eliminated when using TB to obtain SM information [5].

Theoretically, lower frequencies are less attenuated by vegetation and atmosphere, hence the L-band missions such as Soil Moisture and Ocean Salinity (SMOS) and Soil Moisture Active Passive (SMAP) that operate at 1.4 GHz are considered the optimal choice for SM monitoring [3]. However, the spatial resolution is also lower at lower frequencies [7]. The higher multi-frequency passive microwave sensors, such as the Advanced Microwave Scanning Radiometer-Earth Observing System (AMSR-E), and AMSR2, providing a longer sequence of SM observations, which enriched the long-term soil moisture products [2], [6]. The PMV SM retrieval algorithms include the L-band Microwave Emission of the Biosphere (L-MEB) based retrieval algorithm for SMOS [7], the single-channel algorithm (SCA) [8], and the dual channel algorithm (DCA) [9] of SMAP, the Japan Aerospace Exploration Agency (JAXA) algorithm [10], the normalized polarization difference (NPD) algorithm and a LPRM [11] for AMSR-E/2. These algorithms are based on a well-known approximation to the radiative transfer equation, i.e., the τ-ω model [12]. The effective temperature is a crucial parameter in the τ-ω model which needs to be corrected before obtaining reliable SM retrievals [5]. In most studies (including the forward modeling and inversion), it is assumed that the Tv and Ts are approximately equal to a single surface effective composite temperature (i.e., $Tg \approx Tv \approx Ts$) [12]-[14]. This assumption is based on the premise that soil, vegetation canopy, and near-surface air temperature are in relative thermal equilibrium. Generally, most PMW SM retrieval algorithms only use a single effective temperature value to reduce unknown parameters to alleviate the ill-posed problems, ignoring the difference of vegetation and soil temperatures [6], [8]-[11], [13]- [14], even when the difference of soil and vegetation physical temperatures is large, e.g., at AMSR2 ascending overpass (1:30 p.m. local solar time) [15]-[16]. In other words, especially for daytime, most existing AMSR-E/2 SM retrieval algorithms (such as LPRM, JAXA, SCA, NPD, etc.) have neglected the large difference of soil and vegetation physical temperatures over heterogeneity areas, which can bring some uncertainties in the SM estimates [13]. Combined with AMSR-E, the AMSR2 product will facilitate long-term SM monitoring, however, before this can be done, it is necessary to develop a model for temperature decomposition

This work was supported in part by the National Natural Science Foundation of China under Grant 42071346 and Grant 41971317, and in part by the Postgraduate Research & Practice Innovation Program of Jiangsu Province (KYCX22_0661). *(Corresponding author: Yingbao Yang.)*

Xiangjin Meng, Yingbao Yang, and Jia Hu are with the School of Earth Sciences and Engineering, Hohai University, Nanjing 211100, China (e-mail: gisermeng@hhu.edu.cn; yyb@hhu.edu.cn; jiahu@hhu.edu.cn)

Jiangyuan Zeng is with the State Key Laboratory of Remote Sensing Science, Aerospace Information Research Institute, Chinese Academy of Sciences, Beijing 100101, China (e-mail: zengjy@radi.ac.cn).

Jian Peng is with the Department of Remote Sensing, Helmholtz Centre for Environmental Research-UFZ, 04318 Leipzig, Germany, and also with the Remote Sensing Centre for Earth System Research, Leipzig University, 04109 Leipzig, Germany (e-mail: jian.peng@ufz.de).

This article has been accepted for publication in IEEE Geoscience and Remote Sensing Letters. This is the author's version which has not been fully edited and content may change prior to final publication. Citation information: DOI 10.1109/LGRS.2022.3218518

to obtain more reliable SM retrievals in high heterogeneity areas. Among the AMSR-E/2 SM retrieval algorithms, LPRM attempts to solve for SM and vegetation optical depth (VOD) at 10.7 GHz (X band), 6.9 GHz (C1 band), and 7.3 GHz (C2 band) [11]. JAXA retrieves SM and VOD based on a look-up table (LUT) approach [10]. NPD uses the microwave polarization difference (MPD) and a combined vegetation/ roughness factor, and SCA uses normalized difference vegetation index (NDVI) climatology for vegetation correction [17]. Unlike other algorithms, LPRM achieves both retrieval of SM and physical temperature with the least dependence on auxiliary data [18]. Therefore, it is necessary to investigate the inversion uncertainty caused by differences in vegetation and soil temperature in LPRM to improve its applicability.

The purpose of this study is to develop a soil and vegetation temperature decomposition method to improve the original LPRM algorithm, which is expected to improve the accuracy of SM estimations. We tested this new algorithm by using AMSR2 observations and validated it by *in-situ* data collected from three dense soil moisture networks in the TP. The accuracy of soil moisture retrieved from the new algorithm and from the original LPRM was also compared.

II. Study Area and Data

A. Study area

In this study, the TP was selected as the study area (Fig. 1). As the highest plateau in the world, TP is located in the hinterland of Asia, and its mean elevation is more than 4000 m. The TP area has a large diurnal temperature difference, mildly cool and rainy summers, cold and dry winters, and strong winds [19]. SM plays a key role in the energy and water cycles of this area, affecting the Asian monsoon. Three soil moisture networks (Maqu, Naqu, and Ngari) built in the TP were used [20], shown in Fig.1, and their information is listed in Table I.

B. Data

Datasets used in this study include AMSR2 C/Ka-band TB, MODIS NDVI, and SM observation from three densely-instrumented networks (i.e., Maqu, Naqu, and Ngari). The AMSR2 sensor is onboard the GCOM-W1 satellite launched in May 2012. As the successor of AMSR-E, AMSR2 provides an improved calibration system with an additional 7.3 GHz channel and a larger reflector compared to its predecessor for radio frequency interference (RFI) mitigation [21]. Furthermore, previous studies have demonstrated that the TB at C-band (6.9 GHz) was nearly unaffected by RFI over the TP [6], and thus the effects of RFI at the C-band on SM retrieval from AMSR2 are almost negligible in this region. The MODIS/Terra NDVI 16-day/0.05 °product (MOD13C2 v006) was used to calculate fractional vegetation cover (FVC). Refer to [22] for the calculation method of FVC, which is one of the most recognized FVC calculation methods. The FVC was further aggregated to a resolution of 0.1 °that matches AMSR2 pixels in this study. The MODIS/Aqua land surface temperature (LST) daily/0.05 ° product (MYD11C3 v006) was also used to evaluate the temperature of Ts and Tv based on SVTD. Validating microwave-derived temperatures with MODIS LST reference has been adopted by many previous studies (e.g., [23]). In this study, the specific operation is as follows, assuming that in the AMSR2 coarse grid (0.1 °), the fine grid (0.05 °) with MODIS NDVI value less than 0.2 is regarded as pure bare soil pixels, and the ones greater than 0.6 is regarded as pure vegetation pixels. By doing so, the corresponding temperatures can represent the soil surface temperature (SST) and the vegetation canopy temperature (VCT), respectively. The average temperature of all MODIS pure bare soil temperature (called MODIS Tv) or vegetated temperature (called MODIS Tv) grids in the AMSR2 grid can correspond to the Ts and Tv of SVTD respectively. The aggregated average value of all MODIS grids of effective surface temperature (e.g., MODIS LST) in the AMSR2 grid corresponds to the AMSR2 temperature (LPRM-based LST). According to this criterion, a series of valid verification pixels in the study area can be selected after removing the invalid cloud pollution pixels. Additionally, measurements from three dense networks (i.e., Maqu, Naqu, and Ngari) from the International Soil Moisture Network (ISMN) [24] were used to assess the accuracy of SM retrievals. The mean SM was adopted when multiple sites are in one AMSR2 pixel, which can reduce the uncertainty resulting from the spatial mismatch between the *in-situ* point and satellite pixel [25]. Using the newly proposed retrieval algorithm, SM was retrieved from 0.1 °daily ascending (13:30., daytime) and descending (01:30, nighttime) AMSR2 PMW level 3 TB data. Note the frozen period was not considered in this study due to the large uncertainty of soil moisture retrievals during this time. The frozen period is defined as the site soil temperature below 0 ℃, and therefore the frozen period is not the same for each site area. Normally, the frozen period is from November to April of the following year in the study area.

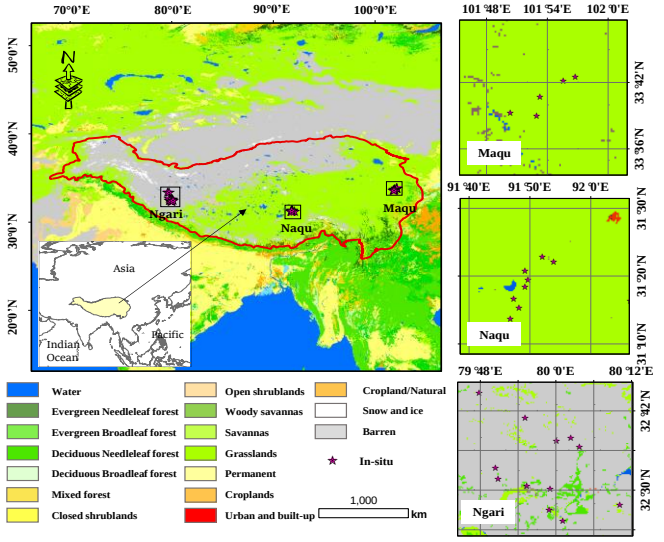

Fig.1. The study area and distribution of *in-situ* sties (red stars) from three networks (Maqu, Naqu, and Ngari). The land cover is derived from the MODIS IGBP land cover classes.

TABLE I
MAIN INFORMATION OF THE THREE SOIL MOISTURE NETWORKS USED IN THE STUDY

Networks	Sites	Depth used (cm)	Mean NDVI*	Land cover	Acquisition time range
Maqu	7	5	0.516	Grasslands	2017.04.01-2019.08.31

Naqu	9	0-5	0.329	Grasslands	2017.04.01-2019.08.31
Ngari	12	0-5	0.118	Barren and grasslands	2017.04.01-2019.06.31

* Annual average NDVI in unfrozen season during the study period.

III. METHODOLOGY

A. Soil-Vegetation Temperature Decomposition (SVTD) Model

Given the actual temperature distribution in the weighted area with respect to the land cover, the mixed canopy temperature measured by the satellite can be computed as follows:

$$Ta(i,j) = \sum_{x=1}^{X} Px(i,j)Tx(i,j) \quad (1)$$

where Ta represents the mixed temperature value; Px and Tx represent the proportion and temperature of the *x-th* type of land surface cover, respectively; X is the number of all land types in the pixel; i,j are the row and column where the pixel is located.

The LPRM surface temperature (ST) was estimated by Holmes et al. (2009) [26] using an empirical model established by Ka-band (37 GHz) V-pol TB and ground-based observations from the United States and several European countries. According to the actual situation of SM inversion, the effective pixel temperature can be simplified as the linear sum of the vegetation component and soil component temperature (water body and urban have been masked), as follows:

$$T_g(i,j) = P_v(i,j)T_v(i,j) + P_s(i,j)T_s(i,j) + \varepsilon \quad (2)$$

where $T_g$represents the effective temperature of the mixed pixel; $T_v$and $T_v$represent vegetation component temperature and soil component temperature, respectively; P_v and P_s represent the proportion of vegetation component and soil component, respectively, and ε represents the model errors.

Here, Pv is defined by FVC, according to [22] using MODIS NDVI, and subject to:

$$P_v(i,j) + P_s(i,j) = 1 \quad (3)$$

Mathematically, equation (2) has infinite solutions, realistic or not. Considering the spatial correlation of temperature pixels, the T_v within neighboring areas can be reasonably assumed to have approximately the same temperature (the same is true for T_s) [27]. Furthermore, the $m\times n$ mixed pixels were selected as a sliding window. Therefore, we can get an equation set consisting of $m\times n$ equation (2) if it is assumed that the $m\times n$ neighboring pixels' component temperatures are consistent, which can be considered as a constrained overdetermined system of linear equations. Considering the size of the microwave pixel, the window should not be too large, and we set m=3 and n=3. The least-square minimizers $\check{\boldsymbol{T}}$ were considered to be constrained as follows:

$$\check{T} = argmin\|Y - PT\| \quad (4)$$

where $\boldsymbol{Y} = [T_g]$ represents the mixed pixel effective temperature vector; $\boldsymbol{T} = [T_v\ T_s]$, T_v and T_s represent the vegetation component effective temperature and soil component effective temperature vectors, respectively; and $\boldsymbol{P} = [P_s\ P_v]$ represent the proportion of vegetation component and soil component vectors, respectively.

The temperature (including vegetation and soil) should vary to a certain extent. According to [28], within a certain range of study area, a scatterplot of the temperature and vegetation index (e.g., NDVI) often results in a triangular or trapezoid shape, that is to say, all the points corresponding to vegetation and temperature are triangles or trapezoids on two-dimensional coordinates (FVC of the *x*-axis data were calculated from vegetation index, *y*-axis data were directly obtained from a local-scale LPRM temperature). Following this concept, the temperatures range corresponding to high and low FVC values can be easily obtained in the scatter triangle (trapezoid). We intercept the interval according to the FVC values statistical histogram. It is regarded as "pure soil" when FVC values is less than 5%, and the corresponding temperature is the soil temperature. Conversely, when the FVC value is greater than 95%, the point (pixel) is regarded as "pure vegetation", and the corresponding temperature is the vegetation temperature. Otherwise, the point (pixel) is regarded as a "soil-vegetation mixture". The average value T_{Mean}, maximum value T_{Max}, minimum value T_{Min}, and standard deviation (STD) value T_{Std} are calculated for the pixels of vegetation and soil range. The optimal solution, namely $\check{\boldsymbol{T}}$, the temperature of vegetation and soil should satisfy the following conditions:

$$T_{Min(v)} - T_{Std(v)} < T_v < T_{Max(v)}T_{Std(v)} \quad (5)$$

$$T_{Min(s)} - T_{Std(s)} < T_s < T_{Max(s)}T_{Std(s)} \quad (6)$$

and

$$\check{T} \in T \quad (7)$$

The optimal solution is required to satisfy both (5), (6) and (7) constraints. To ensure the accuracy of the solution, it is also necessary to design an objective function as a criterion for judging the pros and cons of possible solutions. Select F as the objective function, ξ is a given threshold, and the value depends on the requirements for the expected accuracy. Previous studies have shown that a temperature error of less than 2K has little effect on the accuracy of soil moisture inversion [4], therefore, ξ is set as 2K in this study. The objective function *F* is defined as:

$$F=\sum_{i}^{m}\sum_{j}^{n}\sqrt{(T_g(i,j) - P_v(i,j)T_v(i,j) - P_s(i,j)T_s(i,j))^2} < \xi \quad (8)$$

where $T_g(i,j)$, $T_v(i,j)$, $P_s(i,j)$, $P_v(i,j)$ are as defined in equation (2). Only the decomposition results that satisfy the F test are considered to reduce the illegal error that may be caused by numerical calculation.

B. Soil Moisture Retrieval Model

The SM retrieval algorithm is based on a zero-order radiative transfer model, usually called the τ–ω mode [12], which can be written as follows:

$$T_{b(p)} = (1 - R_{s(p)})T_s\, exp(\frac{-\tau_p}{cos\, u}) + R_{s(p)}\, exp(\frac{-\tau_p}{cos\, u})$$
$$T_v(1 - \omega_p)(1 - exp(\frac{-\tau_p}{cos\, u})) \quad (9)$$

where T_b represents the TB, the subscript p denotes vertical (V) or horizontal (H) polarization, T_v and T_s are the same as in equation (2), τ is the VOD, ω_p is the single scattering albedo of vegetation, u is the satellite incidence angle, R_s represents the soil effective reflectivity as:

$$R_{s(p1)} = (Qr_{s(p2)} + (1-Q)r_{s(p2)})\, exp(-h\cos u) \quad (10)$$

where Q represents the polarization mixing factors, h is the effective roughness parameter, r_s is the smooth surface reflectivity calculated from the Fresnel equations, $p1$ and $p2$ are the opposite polarization (V or H). Hence, the r_s is determined only by the dielectric constant when u is fixed.

Several dielectric mixing models have been developed to describe the relationship between the dielectric constant and SM. Following the LPRM, Wang and Schmugge model [29] was used. LPRM uses an internal analytical method to solve for the VOD and makes use of the Microwave Polarization Difference Index (MPDI) to obtain VOD. In this study, we obtained SM following the same strategy adopted in the LPRM algorithm. The main difference between the proposed SM algorithm and the LPRM algorithm is that an SVTD method was used to isolate the thermal contributions from soil and vegetation.

IV. Results and Discussion

By using the proposed SVTD method, the mixed LPRM temperature was decomposed into the soil and vegetation component temperature. We apply three statistical indicators, namely root mean square error (RMSE), bias, and Pearson correlation coefficient (R) to examine the performance of the SVTD result. The corresponding cross-validation statistics from both the LPRM and SVTD, against MODIS temperature, are reported in Table II. Before decomposition, the agreement between LPRM ST and MODIS LST was high, with stronger agreement at nighttime compared to that at daytime. After decomposition, our proposed method works well in vegetation and bare soil areas during both daytime and nighttime. The performance of SVTD in both vegetation areas and bare soil areas is improved by taking MODIS Tv and MODIS Ts as the references, respectively. Firstly, taking MODIS Tv as the reference, the R-value of SVTD improved by 0.13 and 0.11, and RMSEs of SVTD reduced by 4.39 K and 3.96 K compared with the original LPRM ST in vegetation areas at the daytime and nighttime, respectively (R in SVTD Tv and original LPRM ST at daytime/nighttime are: 0.94/0.96 and 0.81/0.85 respectively; RMSEs in SVTD Tv and original LPRM ST at daytime/nighttime are: 3.11 K/2.70 K and 7.50 K/6.66 K respectively). Secondly, taking the MODIS Ts as the reference, the R-value of SVTD improved by 0.13 and 0.09, and RMSEs of SVTD were reduced by 5.02 K and 3.33 K in bare soil areas compared with LPRM at daytime and nighttime, respectively (R in SVTD Ts and original LPRM ST at daytime/nighttime are: 0.95/0.96 and 0.82/0.87 respectively; RMSEs in SVTD Ts and original LPRM ST at daytime/nighttime are: 4.01 K/2.18 K and 9.03 K/5.51 K respectively).

TABLE II
Error Statistics on the Cross-Comparison Validation of the AMSR2 LPRM and STVD Temperature with MODIS LST (The R are All Significant at p-value < 0.01, the Unit of Bias and RMSE are in K)

Parameters	Day			Night		
	R	Bias	RMSE	R	Bias	RMSE
MODIS LST *vs.* LPRM ST	0.92	4.04	5.51	0.96	-1.07	2.69
MODIS Tv *vs.* LPRM ST	0.81	6.31	7.50	0.85	3.49	6.66
MODIS Tv *vs.* SVTD Tv	0.94	2.77	3.11	0.96	0.96	2.70
MODIS Ts *vs.* LPRM ST	0.82	6.69	9.03	0.87	2.32	5.51
MODIS Ts *vs.* SVTD Ts	0.95	2.28	4.01	0.96	0.62	2.18
N		1118			972	

To evaluate the performance of the proposed algorithm, the three *in-situ* SM networks were used. Fig. 2 (a) and (b) illustrate the comparison of *in-situ* SM and SM retrievals using the proposed algorithm (SVTD SM) and original LPRM in three SM networks at daytime and nighttime, respectively. Both the LPRM SM and SVTD SM have significant overestimation compared to *in situ* measurements in the study area, which is consistent with previous studies [25]. However, the new SVTD SM is closer to the 1:1 line and presents a much better fit to *in situ* data than the original LPRM SM. The SVTD SM also shows more significant improvement compared to LPRM SM in the daytime than in the nighttime. This is in line with expectations since the difference between soil and vegetation is larger in the daytime than at nighttime.

The detailed error statistics of the LPRM and SVTD results are listed in Table III, which demonstrates that the SVTD algorithm has better performance than LPRM by showing a higher R, and smaller bias and unbiased RMSE (*ub*RMSE). Generally, the accuracy of both LPRM SM and SVTD SM is poor in the Maqu network with an *ub*RMSE larger than 0.09 m^3 m^{-3}. The larger error in the Maqu region may be due to the limited penetration of the C-band TB since previous studies reported that the vegetation coverage is the highest in Maqu compared to Naqu and Ngari [20], [25] (this can be also observed in Table I).

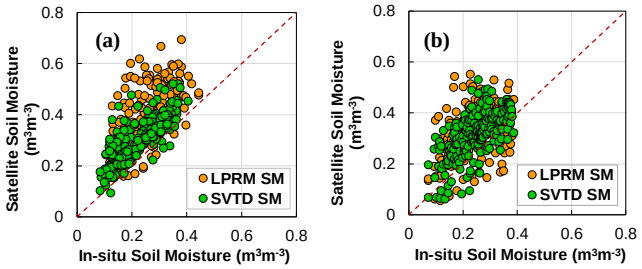

Fig.2. Scatterplots of station-averaged SM and SM retrievals using the proposed algorithm and LPRM algorithm at (a) daytime, and (b) nighttime. The red-dotted diagonal is the 1:1 line.

TABLE III
Performance Metrics of the LPRM SM and SVTD SM for the Unfrozen Seasons in the Three Networks (R are All Significant at 0.01)

Statistic metrics		Maqu		Naqu		Ngari	
		D	N	D	N	D	N
R	LPRM SM	0.306	0.398	0.628	0.696	0.218	0.446
	SVTD SM	0.516	0.584	0.832	0.824	0.423	0.501
Bias (m^3m^{-3})	LPRM SM	0.177	0.114	0.150	0.127	0.168	0.116
	SVTD SM	0.163	0.128	0.121	0.108	0.155	0.104
*ub*RMSE (m^3m^{-3})	LPRM SM	0.111	0.113	0.061	0.078	0.054	0.085
	SVTD SM	0.091	0.095	0.030	0.066	0.047	0.079
N	LPRM SM SVTD SM	406	326	336	356	235	184

Note: D means daytime and N means nighttime

The best performance of both SVTD SM and LPRM SM is obtained in the Naqu network. Generally, the SM estimated from the proposed SVTD algorithm performs better than LPRM SM in all networks, particularly during the daytime, in line with Fig. 2. The most significant improvement appears in the

daytime of the Naqu network (*ub*RMSE reduces from 0.061 to 0.030 m^3m^{-3}, and *R* increases from 0.628 to 0.832), and the Maqu network exhibits a slight improvement in the daytime (*ub*RMSE reduces from 0.111 to 0.091 m^3m^{-3}, and *R* increases from 0.306 to 0.516). Compared with the other two networks, SVTD SM retrievals have a relatively low improvement in the Ngari network both in the daytime (*ub*RMSE from 0.054 to 0.047 m^3m^{-3}, and *R* from 0.218 to 0.423,) and nighttime (*ub*RMSE from 0.085 to 0.079 m^3m^{-3}, and *R* from 0.446 to 0.501). The SVTD method implements based on vegetation coverage, and Maqu is covered with relatively dense vegetation, Naqu is covered with medium vegetation, and Ngari is covered with sparse or even no vegetation (as shown in Table I). From the results, it can be observed that compared to LPRM SM, the performance of SVTD SM is better in the area with relatively moderate vegetation coverage (i.e., Naqu) than in very sparsely vegetated regions (Ngari) and densely vegetated areas (Maqu), and the improvement is stronger at daytime than at nighttime. This also demonstrates the application potential of SVTD in soil vegetation-mixed areas. Based on the SVTD proposed in this study, it can not only avoid using auxiliary data to the greatest extent but also avoids soil moisture inversion errors caused by vegetation soil-temperature differences.

V. Conclusion

In this study, an SVTD method was employed to separate the thermal contributions from soil and vegetation to avoid the assumption made in the PMW SM retrieval algorithms that vegetation and soil temperatures are equal, and thus reduce the uncertainties in soil moisture retrievals, particularly in soil-vegetation mixed regions at daytime. The results indicate that the proposed algorithm is superior to the widely used LPRM algorithm by using *in situ* measurements from three dense networks (Maqu, Naqu, and Ngari) covering different vegetation conditions over TP. Particularly, the proposed algorithm displays a substantial improvement compared to LPRM in moderately vegetated areas during the daytime. The reason is that it employs the new SVTD to decompose vegetation and soil temperatures in mixed pixels using vegetation cover information. It indicates that the existing LPRM temperature model is significantly impacted by the surface vegetated condition and that this impact can be lessened by adopting the SVTD approach, which can improve the accuracy of the SM retrievals.

It is important to note that this study only examines the improvement effect of vegetation differences in various spatial locations on the model and that the vegetation in the same area may change over time. This suggests that much work needs to be done on the evaluation of SVTD suitability during vegetation growth, especially in temperate vegetation areas with significant seasonal changes. To our knowledge, our study is the first attempt to separate the contribution of soil and vegetation temperatures in the passive microwave soil moisture retrieval algorithms using only remote sensing data (that is to say, no model simulations are used in the algorithm to form a purely satellite-dependent dataset). Although SVTD is just tested for AMSR2 data, it has good potential to extend to other multiband PMW satellites such as FY-3C.

References

[1] N. Efremova, M. E. A. Seddik and E. Erten, "Soil Moisture Estimation Using Sentinel-1/-2 Imagery Coupled with CycleGAN for Time-Series Gap Filing," *IEEE Trans. Geosci. Remote Sens.*, vol. 60, pp. 1-11, Art no. 4705111, 2022

[2] S. Kim *et al.*, "A global comparison of alternate AMSR2 soil moisture products: Why do they differ?" *Remote Sens. Environ.*, vol. 161, pp. 43-62, 2015.

[3] J. P. Wigneron *et al.*, "Modelling the passive microwave signature from land surfaces: A review of recent results and application to the L-band SMOS & SMAP soil moisture retrieval algorithms," *Remote Sens. Environ.*, vol. 192, pp. 238-262, 2017.

[4] J. Shi *et al.*, "Microwave vegetation indices for short vegetation covers from satellite passive microwave sensor AMSR-E," *Remote Sens. Environ.*, vol. 112, no. 12, pp. 4285-4300, 2008.

[5] E. G. Njoku *et al.*, "Soil moisture retrieval from AMSR-E," *IEEE Trans. Geosci. Remote Sens.*, vol. 41, no. 2, pp. 215-229, 2003.

[6] J. Zeng *et al.*, "Method for Soil Moisture and Surface Temperature Estimation in the Tibetan Plateau Using Spaceborne Radiometer Observations," *IEEE Geosci. Remote Sens. Lett.*, vol. 12, no. 1, pp. 97-101, 2015.

[7] J. P. Wigneron *et al.*, "L-band Microwave Emission of the Biosphere (L-MEB) Model: Description and calibration against experimental data sets over crop fields," *Remote Sens. Environ.*, vol. 107, no. 4, pp. 639-655, 2007.

[8] T. J. Jackson *et al.*, "III. Measuring surface soil moisture using passive microwave remote sensing," *Hydrol. Process.*, vol. 7, 139–152, 1993.

[9] M. J. Chaubell et al., "Improved SMAP Dual-Channel Algorithm for the Retrieval of Soil Moisture," IEEE Trans. Geosci. Remote Sens., vol. PP, no. 99, pp. 1-12, 2020.

[10] T. Koike *et al.*, "Development of an Advanced Microwave Scanning Radiometer (AMSR-E) Algorithm for Soil Moisture and Vegetation Water Content," *Proc. Hydraul. Eng.*, vol.48, pp.217–222, 2004.

[11] M. Owe, R. D. Jeu, and T. Holmes, "Multi-sensor historical climatology of satellite-derived global land surface moisture," *J. Geophys. Res.*, vol. 113, no. F1, 2008.

[12] T. Mo *et al.*, "A model for microwave emission from vegetation-covered fields," *J. Geophys. Res. -Oceans*, vol. 87, no. C13, pp. 11229–11237, 1982.

[13] Y. H. Kerr *et al.*, "The SMOS Soil Moisture Retrieval Algorithm," *IEEE Trans. Geosci. Remote Sens.*, vol. 50, no. 5, pp. 1384–1403, 2012.

[14] A.Y. Basharinov, and A. Shutko, "Simulation studies of the SHF radiation characteristics of soils under moist conditions," *NASA Tech. Transl.*, vol. TT F-16, 1975.

[15] K. Imaoka *et al.*, Global Change Observation Mission (GCOM) for Monitoring Carbon, Water Cycles, and Climate Change, *Proc. IEEE*, 2010, vol.98, p.5, pp.717-734.

[16] Z. Bian et al., "Retrieving Soil and Vegetation Temperatures from Dual-Angle and Multipixel Satellite Observations," *IEEE J Sel. Top. Appl. Earth Obs. Remote Sens*. vol. 13, pp. 5536-5549, 2020

[17] Y. Gao *et al.*, "Multi-frequency radiometer-based soil moisture retrieval and algorithm parameterization using in situ sites," *Remote Sens. Environ.*, vol.279, pp.15, 2022.

[18] R. Bindlish, *et al.*, "GCOM-W AMSR2 Soil Moisture Product Validation Using Core Validation Sites," *IEEE J Sel. Top. Appl. Earth Obs. Remote Sens.*, vol.11, p.99, pp.209-219, 2018.

[19] J. Peng *et al.*, "Comparison of satellite-based evapotranspiration estimates over the Tibetan Plateau," *Hydrol. Earth Syst. Sci.*, vol. 20, no. 8, pp. 316-3182, 2016.

[20] Z. Su *et al.*, "The Tibetan Plateau observatory of plateau scale soil moisture and soil temperature (Tibet-Obs) for quantifying uncertainties in coarse resolution satellite and model products," *Hydrol. Earth Syst. Sci.*, vol. 15, no. 7, pp. 2303, 2017.

[21] R. A. M. De Nijs *et al.*, "A Methodology to Determine Radio-Frequency Interference in AMSR2 Observations," *IEEE Trans. Geosci. Remote Sens.*, vol. 53, no. 9, pp. 5148-5159, 2015.

[22] D. Chu, Fractional Vegetation Cover: Remote Sensing of Land Use and Land Cover in Mountain Region: A Comprehensive Study at the Central Tibetan Plateau., 2020.

[23] Song *et al*., "An Improved Soil Moisture Retrieval Algorithm Based on the Land Parameter Retrieval Model for Water–Land Mixed Pixels Using AMSR-E Data," *IEEE Transactions on Geoscience and Remote Sensing*, vol. 57, no. 10, pp. 7643-7657, 2019

[24] W. A. Dorigo *et al.*, "The International Soil Moisture Network: a data hosting facility for global in situ soil moisture measurements," *Hydrol. Earth Syst. Sci.*, vol. 15, no. 5, pp. 1675-1698, 2011.

[25] J. Zeng *et al.*, "Assessment and Error Analysis of Satellite Soil Moisture Products Over the Third Pole," *IEEE Trans. Geosci. Remote Sens.*, vol. 60, pp. 1-18, 2022.

[26] T. R. H. Holmes *et al.*, "Land surface temperatures from Ka-band (37 GHz) passive microwave observations". *J. Geophys. Res.*, vol. 114, no. D4, Art. no. D04113, 2009.

[27] L. Gu, R. Ren, and X. Li, "Snow Depth Retrieval Based on a Multi-frequency Dual-Polarized Passive Microwave Unmixing Method from Mixed Forest Observations," *IEEE Trans. Geosci. Remote Sens.*, vol. 54, pp. 7279-7291, 2016.

[28] T. N. Carlson, R. R. Gillies, and E. M. Perry, "A method to make use of thermal infrared temperature and NDVI measurements to infer surface soil water content and fractional vegetation cover," *Remote Sens. Reviews*, vol. 9, no. 1-2, pp. 161-173, 1994.

[29] J. R. Wang, and T. J. Schmugge, "An Empirical Model for the Complex Dielectric Permittivity of Soils as a Function of Water Content," *IEEE Trans. Geosci. Remote Sens.*, vol. GE-18, no. 4, pp. 288-295, 1980.